Fluid Dynamics & Materials Processing

Tech Science Press

DOI: 10.32604/fdmp.2023.027877

ARTICLE

Influence of Erosion Induced by NaCl on the Mechanical Performances of Alkali-Activated Mineral Admixtures

Jing Yu[1], Jie Ren[2], Guangming Shen[3], Weixiang Sun[2] and Hui Wang[4,*]

[1]Department of Architectural Engineering, Ningbo Polytechnic, Ningbo, 315000, China

[2]Technology and Performance Management Department, China Construction Infrastructure Corp., Ltd., Beijing, 10029, China

[3]Chief Engineer's Office, Jiuzhou Engineering Design Co., Ltd., Zhengzhou, 451162, China

[4]School of Civil Engineering and Geographic Environment, Ningbo University, Ningbo, 315000, China

[*]Corresponding Author: Hui Wang. Email: huiwang123@aliyun.com

Received: 22 November 2022 Accepted: 20 February 2023 Published: 18 May 2023

ABSTRACT

In this paper, the influence of NaCl freeze-thaw (F-T) cycles and dry-wet (D-W) alternations on the flexural, compressive and bonding strengths of alkali-activated fly ash (FA) and a blast furnace slag powder (BFS) is investigated. The considered NaCl concentration is 3%. The effect of polypropylene fibers on the mechanical strengths is also examined. Scanning electron microscopy (SEM), thermogravimetry (TG) and X-ray diffraction (XRD) are selected to discern the mechanisms underpinning the NaCl-induced erosion. The obtained results indicate that the best results in terms of material resistance are obtained with admixtures containing 60% BFS and 40% FA in terms of mass ratio and 3% polypropylene fibers in terms of volume ratio. The maximum rates of decrease of the flexural, compressive and bonding strengths after 300 NaCl F-T cycles are 21.5%, 20.3% and 22.6%, respectively. The corresponding rates of decrease due to NaCl D-W alternations are 28.1%, 26.1% and 31.5%, respectively. The TG curves show that the alkali-activating activity of BFS is higher than that of FA. Moreover, in the first case, the microstructure of the hydration products is more compact. The results also show that NaCl F-T cycles lead to increasing cracks in the alkali-activated BFS.

KEYWORDS

Mechanical performances; alkali-activated; NaCl dry-wet alternations; NaCl freeze-thaw cycles; microstructure

Abbreviations

F-T	Freeze-Thaw
D-W	Dry-Wet
FA	Fly Ash
BFS	Blast Furnace Slag
SEM	Scanning Electron Microscopy
TG	Thermogravimetry
XRD	X-Ray Diffraction
RPC	Reactive Powder Concrete

1 Introduction

1.1 Research Background

As a transportation hub in coastal cities, cross sea bridges have been built extensively. These building parts usually encounter complex chloride environmental effects. When winter comes, some parts of the cross sea bridges are usually exposed to the freeze-thaw (F-T) cycles of seawater [1–3]. Moreover, when the rise and fall of sea water occur, the dry-wet (D-W) alternations of seawater will erode the cross sea bridges [4–6]. Based on the above reasons, the bridge concrete is frequently damaged.

The damaged bridge concrete is usually repaired with rapid-strength cement concrete material or asphalt concrete material. The sulphoaluminate cement, magnesia-phosphate cement and portland cement with early strength agents have been used to create ingredients for rapid-strength cement concrete [7]. However, the application of cement-based repairing materials has some drawbacks. The sulphoaluminate cement and magnesia-phosphate cement show high costs and are easy to crack. Moreover, the later strength of the sulphoaluminate cement and magnesia-phosphate cement-based materials will be attenuated during service [8–10]. The asphalt mixtures are used for repairing the damaged parts of the bridge deck and the pavement due to the convenience of construction. However, asphalt is expensive and produces toxic and harmful gases during use. Hence, new bridge decks and pavement repairing materials need to be developed [11–14]. As reported in prior researches [15,16], the reactive powder concrete material with sulphoaluminate cement or the assembly unit of sulphoaluminate cement and Ordinary Portland cement show excellent bonding strengths. However, the NaCl action can reduce their bonding strengths by higher than 30%. Therefore, materials with better compactness need to be developed.

1.2 Research Significance

Alkali-activated mineral admixtures have been developed and studied for decades. This kind of material shows high strength and compactness. As reported in prior research that the alkali-activated slag powder shows a compressive strength of higher than 100 MPa and flexural strength of higher than 20 MPa [17–19]. The optimized preparation of alkali-activated slag powder and the corresponding mechanical strengths have been investigated for several years. Mineral additives like fly ash (FA) and blast furnace slag powder (BFS) and stove ashes are cheap and easy to get [20,21]. Several researches have focused on the mechanical performances, the durability and the micro performance of alkali-activated mineral admixtures. Meanwhile, in prior researches, the alkali-activated mineral admixture usually has only one mineral admixture. Compound mineral admixtures usually contain two or more kinds of mineral admixtures. This mixing method can combine the advantages of different admixtures, however, little attention has been paid to this. Peng et al. [22] have reported that the mechanical strengths of the alkali-activated compound mineral admixtures can be effectively improved by the addition of BFS. Meanwhile, the corrosion resistance of reinforced alkali-activated compound mineral admixtures exposed to NaCl action is increased by BFS [23]. However, almost no attention has been concerned to the influence of NaCl action on the mechanical strengths of activated compound mineral admixtures. The innovation of this study is the systematic research of the effects of chloride erosion on the mechanical properties and corresponding micro properties of alkali-activated compound mineral admixtures.

1.3 Research Objective

This study aims to investigate the flexural and compressive strengths of alkali activated compound mineral admixtures. The bonding strength between the alkali-activated compound mineral admixtures and the cement mortar is determined. The specimens are exposed to the F-T cycles and D-W alternations with the NaCl concentration of 3%. Finally, the thermogravimetry (TG) and the scanning electron microscope (SEM) photos are selected for investigating the mechanism of the resistance to NaCl F-T cycles and D-W

alternations. The findings of this study will help develop a new kind of repairing material for bridge deck pavement.

2 Materials and Test Process

2.1 Raw Materials

The sodium silicate with a melting point ranging from 40°C to 48°C provided by Tianjin Zhiyuan Chemical Co., Ltd., Tianjin, China is used for manufacturing the alkali-activated BFS and FA. The density, boiling point and purity of the sodium silicate are 2.13 g/cm^3, 1390°C and 99.9% respectively. The BFS and FA offered by Henan Bairun New Materials Co., Ltd., Gongyi, China, show densities of 2.88 g/cm^3 and 2.4 g/cm^3. While, their ignition losses are 1.03% and 1.975%, respectively. Tables 1 and 2 respectively display the raw materials' particle passing percentage and chemical composition.

Table 1: Particle passing percentage of raw materials (%)

Types	0.3 μm	0.6 μm	1 μm	4 μm	8 μm	64 μm	360 μm
BFS	0.03	0.1	3.5	19.6	35.0	97.9	100
FA	12.3	41.7	66.2	100	100	100	100

Table 2: The chemical composition (%)

Types	SiO_2	Al_2O_3	Fe_xO_y	MgO	CaO	SO_3	K_2O	Na_2O	Ti_2O	LI
BFS	34.1	14.7	0.2	9.7	35.9	0.2	3.5	—	—	—
FA	55.00	20.00	6.00	10.20	4.50	0.11	1.26	2.13	0.06	0.74

2.2 Specimen Preparation

Table 3 shows the mixing proportions of all specimens. The NJ-160A cement paste mixer is used for mixing the alkali-activated FA and BFS. In this study, the water-binder (the mass ratio of water: (FA +BFS+$Na_2O{\cdot}nSiO_2$+NaOH)) ratio is 0.3, which is convenient for comparison with previous studies [24]. The alkali-activated cementitious material is used for manufacturing geopolymer concrete. Firstly, the water, NaOH and $Na_2O{\cdot}nSiO_2$ are mixed in the mixer for 30 s with the mixing speed of 140 r/min, after this mixing, the FA and BFS are added to the mixer, and stirred at 140 r/min for 1.5 min, then stirred for an additional 2 min at 180 r/min. The preparation of specimens is shown in Fig. 1.

Table 3: The mixing proportions (kg/m^3)

Specimens	FA	BFS	Alkali equivalent	W/B	Modulus	$Na_2O{\cdot}nSiO_2$	NaOH
A1	300	0	3%	0.3	1	29.83	6.69
A2	240	60	3%	0.3	1	29.83	6.69
A3	180	120	3%	0.3	1	29.83	6.69
A4	120	180	3%	0.3	1	29.83	6.69
A5	60	240	3%	0.3	1	29.83	6.69
A6	0	300	3%	0.3	1	29.83	6.69

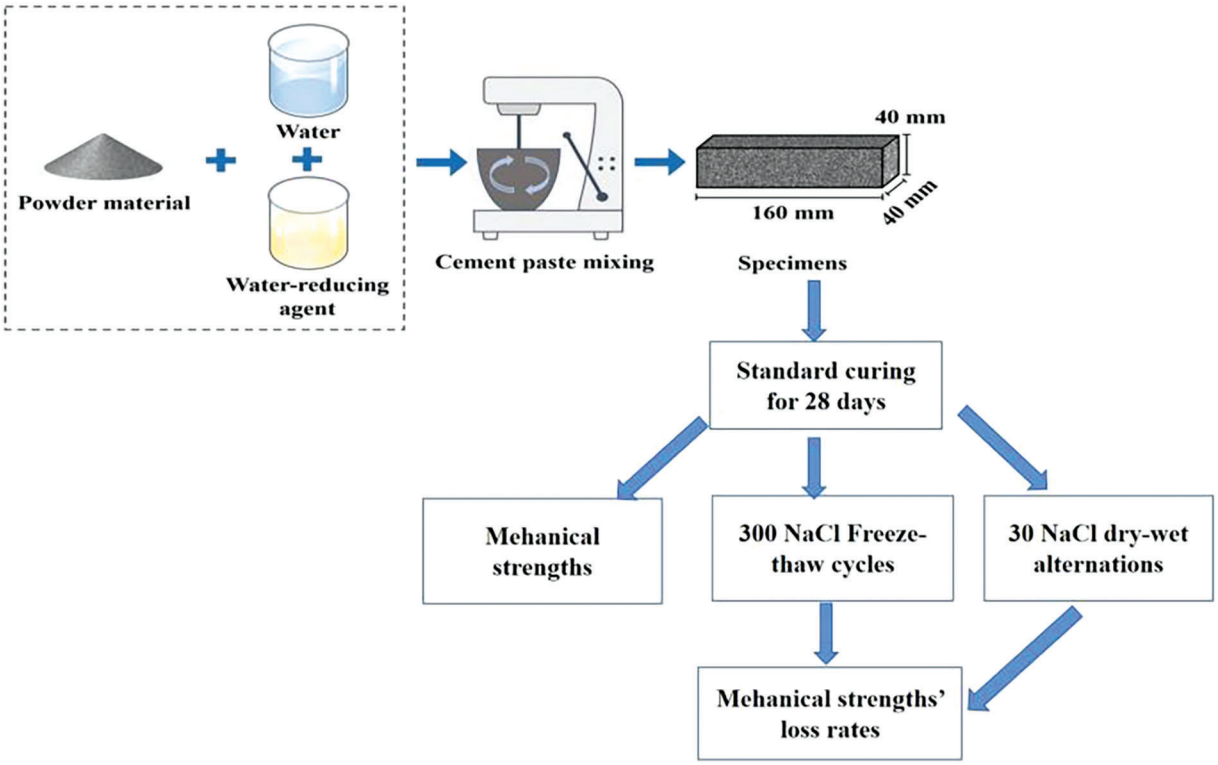

Figure 1: The preparation of specimens

Once the mixing is completed, the fresh alkali-activated compound mineral admixture is poured into the molds with the size of 40 mm^3 × 40 mm^3 × 160 mm^3. After pouring, the specimens are moved to cure in an environment of 20 ± 2°C and relative humidity of 40% for 1 day. Then, all specimens are demoulded and placed in an environment of 20 ± 2°C and 98.3% relative humidity for curing. The modulus of potassium silicate is 1.0. The modulus of potassium silicate means the amount of substance ratio of SiO_2: (K_2O +NaOH). The polypropylene fibers with the density of 0.91 g/cm^3, average length and diameter of 12 mm and 26.1 μm are used in this study. The polypropylene fibers show the tensile strength and average elastic modulus of 710 and 3850 MPa.

2.3 Measurement

2.3.1 Macro Performance

YAW-300C full-automatic bending and compression resistance integrated testing machine is used to measure the mechanical strengths. Flexural and bonding strengths are loaded at a rate of 0.05 kN/s, while, the compressive strength's loading speed is 2.4 kN/s. The maximum compressive and flexural loads of the full-automatic bending and compression resistance integrated testing machine are 300 kN and 10 kN. The specimens are firstly bent to failure and then the two testing blocks of the broken sections are used for the measurement of compressive strength. The testing machine for the flexural and compressive strengths are shown in Fig. 2. The bonding strength is expressed as follows. The cement mortar with the mass ratios of cement: standard sand: water of 1:3:0.3 is used for measuring the bonding strength. The first step is to use the cutting machine to cut the cement mortar in half after it has been curing for 28 days in the standard environment. The half mortar specimen is filled with the fresh alkali-activated

compound mineral admixture and moved to the standard curing environment curing for 1, 3 and 28 days. After curing, all specimens are moved for measuring the bonding strength with the full-automatic bending and compression resistance integrated testing machine. The loading speed is the same as that of the experiment on flexural strength. The experimental sketch for bonding strength is illustrated in Fig. 3. Samples preparation, size and testing are conducted according to the Chinese standard GB/T 17671-1999.

Figure 2: The measurement of mechanical strengths

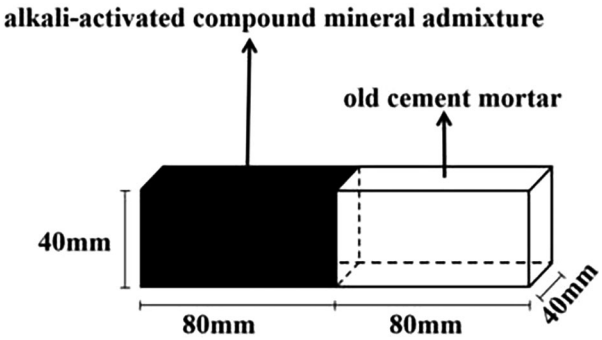

Figure 3: The experimental sketch for bonding strength

The detailed processes of the F-W cycles and D-W alternations with NaCl solution are described as follows.

The specimens with sizes of 40 mm^3 × 40 mm^3 × 160 mm^3 are immersed in the solution with 3% NaCl for 4 days. After the immersion is finished, all specimens are moved to the DR-10A cement automatic quick freezing and thawing machine (Foshan Nanchao E-Commerce Co., Ltd., Foshan, China) and salt spray cyclic corrosion tester (Yangzhou, China) for the experiments of NaCl F-W cycles and D-W alternations, respectively. The temperature of NaCl F-W cycles ranges from −15°C to 8°C. The specimens are immersed in the rubber tubes filled with 3% NaCl solution during the F-W cycles. The humidity and the temperature of the salt spray cyclic corrosion tester are 30%~95% and 47°C~63°C. The experiments of NaCl F-W and D-W alternations are conducted according to Wang's research [25].

2.3.2 Micro Performance

Some samples are crushed into powder and sieved, after that the samples are moved to the thermal analyzer provided by Shandong Longmei Mining Machinery Co., Ltd., Jinan, China, with the temperature ranging from 20°C to 1000°C for the TG analysis experiment. While some other soybean size samples prayed with gold are used for the measurement of SEM.

3 Results and Discussions

3.1 Influence of Mineral Admixtures on Mechanical Strengths

The specimens' flexural, compressive, and bonding strengths are depicted in Fig. 4. It can be observed in Fig. 4, the three types of mechanical strengths increase with the increasing dosages of BFS. Due to the higher content of $[SiO_4]^{4-}$ in FA, the FA possesses polymerization in the vitreous structure network [26,27]. Therefore, the FA shows low alkali-activated activity. As shown in Fig. 4, the growing rates of mechanical strengths of BFS start visibly with the dosages of BFS ranging from 0% to 60%. However, when the mass ratio of BFS increases from 60% to 100%, mechanical strengths grow steadily. Meanwhile, Fig. 4 demonstrates that the increasing rate of the mechanical strengths grows in this order: bonding strength rate > compressive strength rate > flexural strength rate. The errors have all been calculated to be less than 0.1, demonstrating the precision of the study results [28,29].

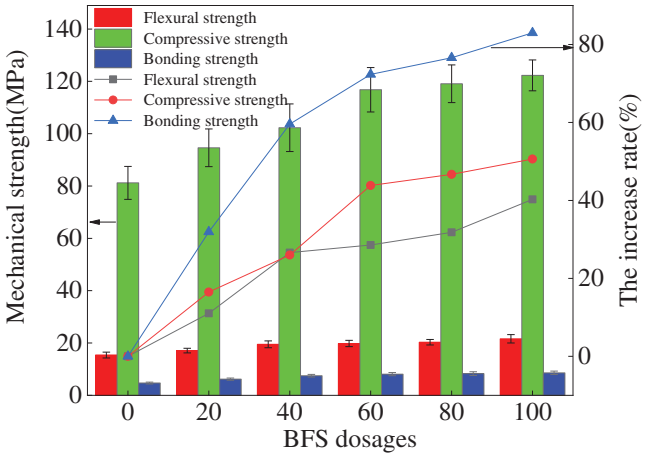

Figure 4: The mechanical strengths of specimens

Fig. 5 shows the loss rates of the mechanical strengths of specimens after exposing to 300 NaCl F-T cycles. As shown in Fig. 5, the mechanical strengths drop clearly with the increasing number of NaCl F-T cycles. This is explained by the ability of the NaCl F-T cycles to widen the internal fissures in reactive powder concrete (RPC), which in turn resulting in declining the mechanical strengths [30]. Additionally, the sodium chloride crystallization stress is caused by the crystallization of sodium chloride during NaCl F-T cycles. Moreover, as depicted in Fig. 5, the increasing dosages of BFS demonstrate the decreasing effect on the loss rates of the mechanical strengths. Additionally, as illustrated in Fig. 5, the error bar values are lower than 0.1, demonstrating great accuracy. Finally, as illustrated in Fig. 5, the mechanical strengths' loss rates decrease in this order: bonding strength rate > compressive strength rate > flexural strength rate.

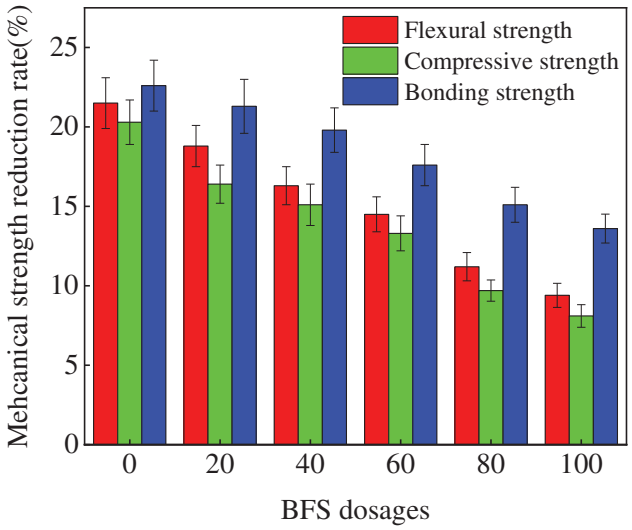

Figure 5: The strengths loss of specimens after NaCl F-T cycles

Fig. 6 depicts the loss rates of the mechanical strengths of the specimens. The mechanical strengths are determined after 30 NaCl D-W alternations. As shown in Fig. 6, the NaCl D-W alternations cause a drop in the mechanical strengths. The reason for this is that when the specimens are dried at high temperatures, sodium chloride crystal precipitation occurs. Meanwhile, when the specimens are laid in NaCl solution, the sodium chloride crystal precipitation disappears. Therefore, the specimens encounter the effect of cyclic crystallization stress leading to the damage in the specimens. Consequently, the NaCl D-W alternations lead to decreasing the mechanical strengths of the specimens. As shown in Fig. 6 that the mechanical strengths' loss rates decrease with the increasing dosages of BFS. It can be obtained from Fig. 6, the loss rates of mechanical strengths decrease in this order: bonding strength rate > flexural strength rate > compressive strength rate [31,32].

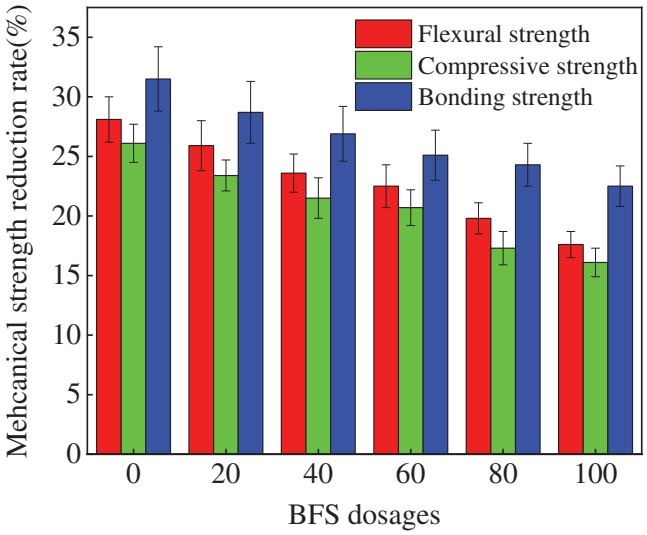

Figure 6: The strengths loss of specimens after NaCl D-W alternations

3.2 Influence of Polypropylene Fibers on Mechanical Strengths

Fig. 7 displays the mechanical properties of the specimens mixed with different volume ratios of steel fibers and polypropylene fibers. As demonstrated in Fig. 7, the mechanical strengths of specimens increase with the increasing dosage of polypropylene fibers. Meanwhile, the increasing rates of mechanical strengths increase. This is ascribed to the fact that the addition of polypropylene fibers has the function of bridging cracks inner the specimens thus improving the mechanical strengths [33]. The increasing rates of the mechanical strengths increase obviously with the volume of fibers ranging from 0% to 2%. Meanwhile, when the volume of polypropylene fibers increases from 2% to 3%, the increasing rates of mechanical strength increase slowly. It can be obtained from Fig. 7, the increasing rates of the mechanical strengths decrease in the order of flexural strength rate > bonding strength rate > compressive strength rate. It can be obtained from Fig. 7, the error bar values are less than 0.1, demonstrating the accuracy of the experimental findings.

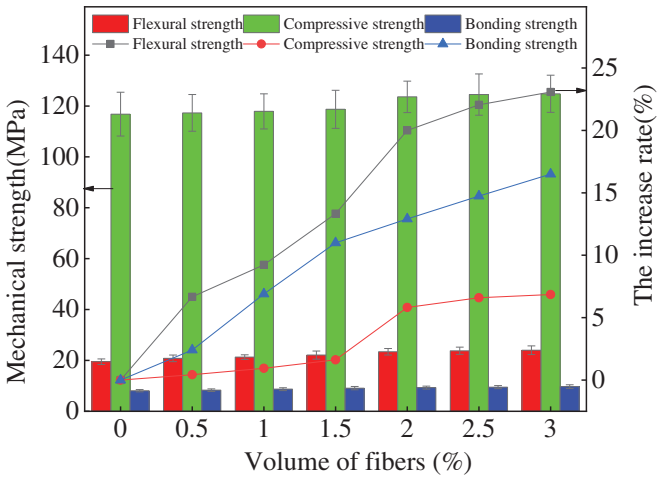

Figure 7: The mechanical strengths of specimens with polypropylene fibers

When the NaCl erosion is exerted on the cement-based materials, the crystallization of sodium chloride will cause cracks inner specimens, which leads to the reduction of mechanical strengths. The alkali-activated compound mineral admixture is a special cement-based material, meanwhile, the effect of NaCl erosion on its mechanical strength is similar to that of normal cement-based material. The mechanical strength reduction rates of the specimens mixed with polypropylene fibers after 300 NaCl F-T cycles are depicted in Fig. 8. As illustrated in Fig. 8, the mechanical strength reduction rates decrease with the increasing dosages of polypropylene fibers. This is ascribed to the fact that polypropylene fibers can effectively limit crack propagation [34]. Therefore, the mechanical strength reduction rates of the specimens decrease with the increasing dosages of polypropylene fibers. The decreasing rates of the mechanical strengths of the polypropylene fibers alkali-activated compound mineral admixtures decrease in this order of bonding strength loss rate > flexural strength loss rate > compressive strength loss rate.

The mechanical strength reduction rates of the specimens mixed with polypropylene fibers after 30 NaCl D-W alternations are depicted in Fig. 9. As illustrated in Fig. 9, the mechanical strength reduction rates decrease with the increasing dosages of polypropylene fibers. This is ascribed to the fact that the increased cracks are prevented by the polypropylene fibers, eventually resulting in increasing the mechanical strengths. Consequently, the mechanical strength loss rates decrease in the order as follows: bonding strength loss rate > flexural strength loss rate > compressive strength loss rate. The error of all Figures are lower than 10% of the experimental values, indicating high accuracy of the results.

Comparing with the normal cement-based materials, the mechanical strength reduction rates are 31.2% ~41.3% and 35.6%~44.5% after 300 NaCl F-W cycles and 30 D-W alternations [24]. Meanwhile, as depicted in this study, the mechanical strength reduction rates are 9.6%~17.3% and 17.6%~25.1% after 300 NaCl F-W cycles and 30 D-W alternations. Researching findings show that the alkali-activated compound mineral admixture shows better resistance to NaCl erosion than that of normal cement-based materials.

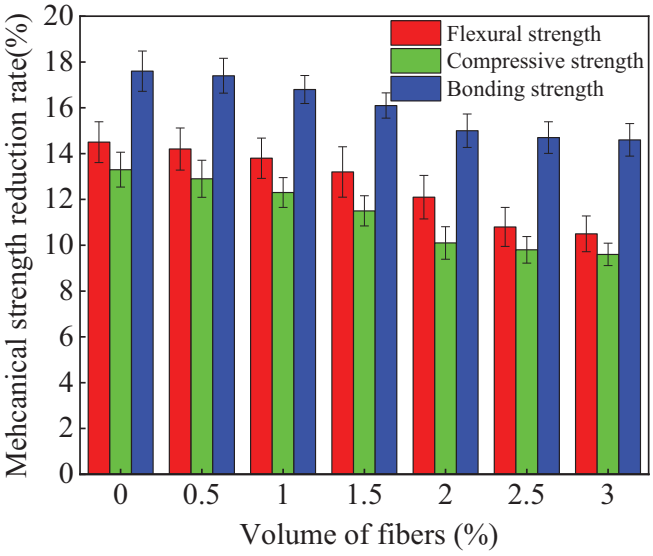

Figure 8: The strengths loss of specimens after NaCl F-T cycles

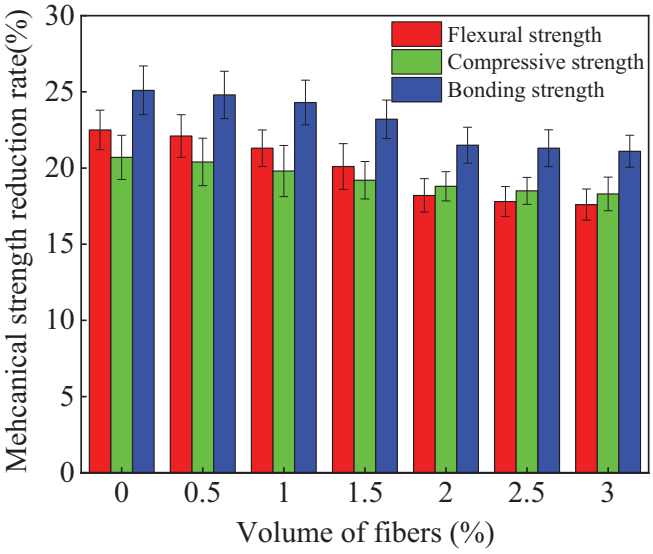

Figure 9: The strengths loss of specimens after NaCl D-W alternations

3.3 The Micro Researching Results

The TG analysis results are exhibited in Fig. 10. In this experiment, the temperature ranges from 29.75°C to 950°C. The samples are the alkali-activated FA, alkali-activated BFS and alkali-activated BFS after 300 NaCl F-T cycles. As demonstrated in Fig. 10, the TG appears in the decreasing trend. The variation of the TG analysis can be divided into three stages. The first stage is the stage with the temperature of 29.75°C to 123.8°C, in this step, the free water evaporates and disappears thus leading to the reduction of the mass of samples. Meanwhile, when the temperature ranges from 123.8°C to 450.51°C, the second stage occurs, in this stage, the reduction of TG occurs, due to hydrotalcite's decomposition thus decreasing the TG. Finally, when the temperature is 450.51°C~900°C, the TG curve firstly decreases obviously and then becomes stable. In this step, the calcium silicate hydrate starts to decompose until finished. As observed in Fig. 8, the addition of FA leads to increasing the TG values, due to the lower alkali activating activity than that of BFS. Moreover, the NaCl F-T cycles demonstrate the decreasing effect on the TG values, because of the continuous hydration during NaCl F-T cycles [35].

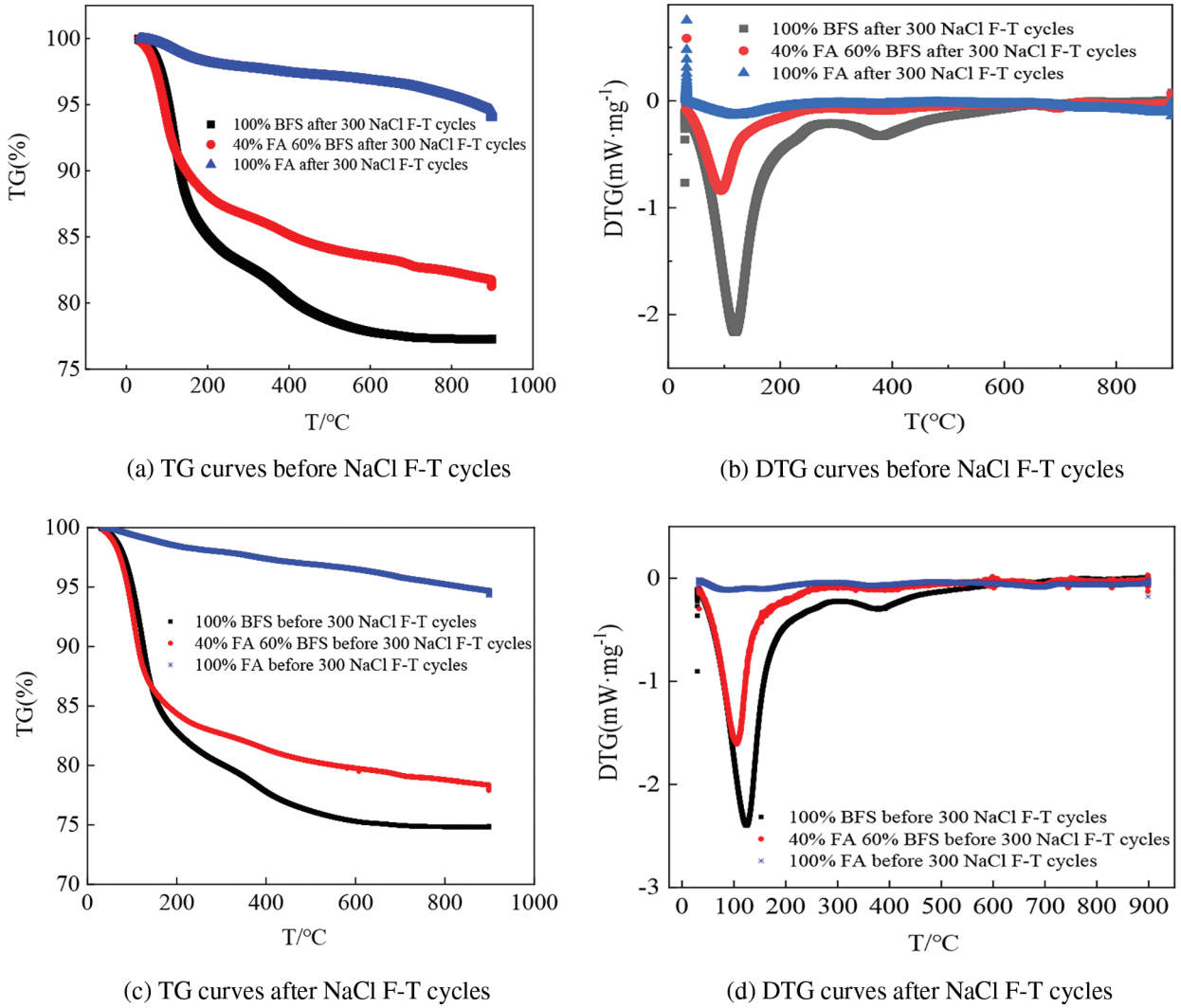

(a) TG curves before NaCl F-T cycles

(b) DTG curves before NaCl F-T cycles

(c) TG curves after NaCl F-T cycles

(d) DTG curves after NaCl F-T cycles

Figure 10: TG analysis curves of specimens

The scanning electron microscopy(SEM) photos of alkali-activated FA and BFS are illustrated in Fig. 11. The specimens are alkali-activated FA, alkali-activated BFS and alkali-activated BFS after 300 NaCl F-T cycles. It can be depicted in Fig. 11, the hydration products of alkali-activated FA are blocky. Moreover, the SEM photo of alkali-activated BFS is more compact than that of alkali-activated FA. Finally, as observed in Fig. 11, more cracks occur in alkali-activated BFS after 300 NaCl freeze-thaw cycles. Therefore, the erosion of chlorine salt can decrease the mechanical strengths of the alkali-activated compound mineral admixture [36–40].

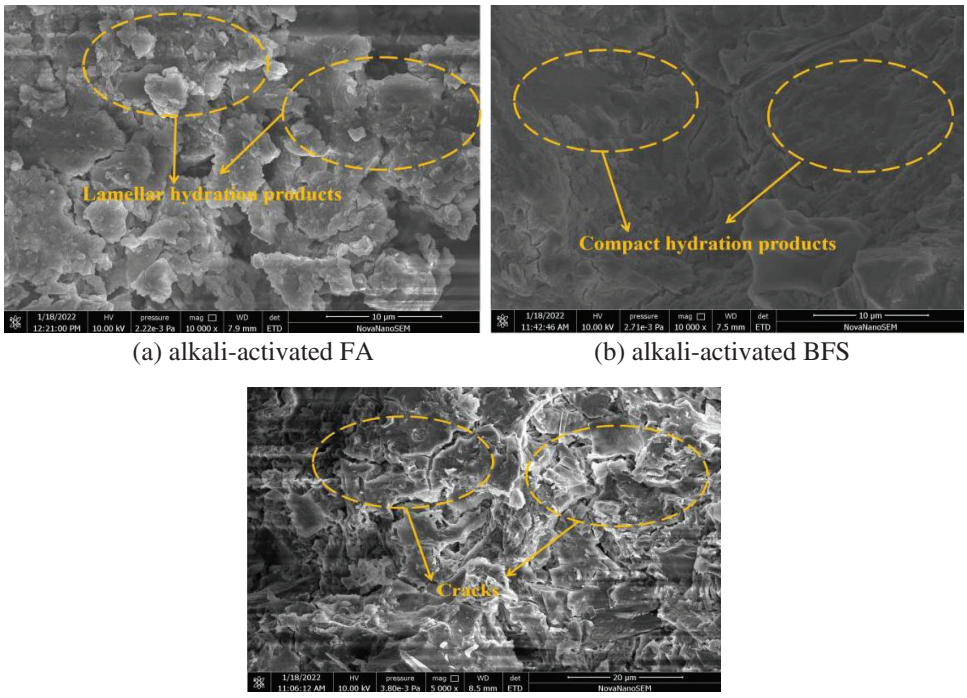

(a) alkali-activated FA (b) alkali-activated BFS

(c) alkali-activated BFS after NaCl F-T cycles

Figure 11: The SEM morphology of alkali-activated FA and BFS

4 Conclusions

The purpose of this study was to examine the effect of NaCl erosion on the mechanical properties and micro-properties of alkali-activated compound mineral admixtures. The following conclusions were drawn:

(a) The addition of BFS improved the mechanical strengths of alkali-activated compound mineral admixtures, with the greatest impact being on bonding strength.

(b) The mechanical strengths of alkali-activated compound mineral admixtures were reduced by NaCl freeze-thaw cycles and dry-wet alternations. The maximum decrease in flexural, compressive, and bonding strengths was 21.5%, 20.3%, and 22.6% due to freeze-thaw cycles, and 28.1%, 26.1%, and 31.5% due to dry-wet alternations. 60% BFS and 40% FA by mass ratio of the total compound mineral admixtures composed with and 3% polypropylene fibers by volume ratio of the total alkali-activated compound mineral admixtures are considered as the mixing proportions in optimal engineering application.

(c) BFS had higher alkali-activating activity than FA, and the hydration products of alkali-activated BFS were more compact than those of alkali-activated FA. However, after 300 NaCl freeze-

thaw cycles, the hydration products of alkali-activated BFS had more cracks than those of alkali-activated FA.

(d) Higher protective measures are needed for the alkali-activated compound mineral admixtures exposing under the NaCl D-W alternations than NaCl F-T cycles in the future.

Acknowledgement: Conceptualization, H.W. and J.Y.; methodology, R.J.; validation, J.Y. and H.W.; formal analysis, J.Y. and H.W.; investigation, J.Y., S.W. and S.G.; resources, R.J.; data curation, H.W. and J.Y.; writing—original draft preparation, H.W. and J.Y.; writing—review and editing, H.W., J.Y., R.J., S.G. and S.W.; visualization, J.Y.; supervision, R.J.; project administration, H.W. and J.Y.; funding acquisition, H.W. and S.W. All authors have read and agreed to the published version of the manuscript.

Funding Statement: This research is supported by 2023 University-Level Scientific Research Project of Ningbo Polytechnic (NZ23002) and the First Batch of Ningbo Construction Scientific Research Projects in 2023 (20230106).

Conflicts of Interest: The authors declare that they have no conflicts of interest to report regarding the present study.

References

1. Shakiba, M., Bazli, M., Karamloo, M., Mortazavi, S. M. R. (2022). Bond-slip performance of GFRP and steel reinforced beams under wet-dry and freeze-thaw cycles: The effect of concrete type. *Construction and Building Materials, 342,* 127916.
2. Pavan Kumar, D., Vinay Babu, S., Surakasi, R., Bradley Bright, B., Rajeeth, T. J. et al. (2022). Influence of nano-filler content on the freeze-thaw cycle of the nano-concrete mixture. *Materials Today: Proceedings, 62(8),* 5164–5168.
3. Haselbach, L., Valavala, S., Montes, F. (2005). Permeability predictions for sand clogged Portland cement pervious concrete pavement systems. *Journal of Environmental Management, 81,* 42–49.
4. Bayraktar, O. Y., Kaplan, G., Benli, A. (2022). The effect of recycled fine aggregates treated as washed, less washed and unwashed on the mechanical and durability characteristics of concrete under $MgSO_4$ and freeze-thaw cycles. *Journal of Building Engineering, 48,* 103924.
5. Ozata, S., Akturk, B., Yuzer, N. (2022). Utilization of waste Cappadocia earth as a natural pozzolan in alkali activation: A parametric study. *Construction and Building Materials, 329,* 127192.
6. Supriya, J., Raut, A. (2021). Performance parameter analysis of magnesia based cement products–A review. *IOP Conference Series: Materials Science and Engineering, 1197,* 012078.
7. Alomayri, T., Adesina, A., Das, S. (2021). Influence of amorphous raw rice husk ash as precursor and curing condition on the performance of alkali activated concrete. *Case Studies in Construction Materials, 15,* e00777.
8. Telesca, A., Marroccoli, M., Coppola, L., Coffetti, D., Candamano, S. (2021). Tartaric acid effects on hydration development and physico-mechanical properties of blended calcium sulphoaluminate cements. *Cement and Concrete Composites, 124,* 104275.
9. Adesina, A. (2020). Recent advances in the concrete industry to reduce its carbon dioxide emissions. *Environmental Challenges, 1,* 100004.
10. Witoon, T., Lapkeatseree, V., Numpilai, T., Cheng, C., Limtrakul, J. (2022). CO_2 hydrogenation to light olefins over mixed Fe-Co-K-Al oxides catalysts prepared via precipitation and reduction methods. *Chemical Engineering Journal, 428,* 131389.
11. Witoon, T., Numpilai, T., Nijpanich, S., Chanlek, N., Kidkhunthod, P. et al. (2022). Enhanced CO_2 hydrogenation to higher alcohols over K-Co promoted In_2O_3 catalysts. *Chemical Engineering Journal, 431,* 133211.
12. AL-Ameeri, A. S., ImranRafiq, M., Tsioulou, O., Rybdylova, O. (2021). Impact of climate change on the carbonation in concrete due to carbon dioxide ingress: Experimental investigation and modelling. *Journal of Building Engineering, 44,* 102594.

13. Kamal, N. L. M., Itam, Z., Sivaganese, Y., Beddu, S. (2020). Carbon dioxide sequestration in concrete and its effects on concrete compressive strength. *Materials Today: Proceedings, 31,* A18–A21.
14. Egodagamage, H., Yapa, H. D., Samith Buddika, H. A. D., Navaratnam, S., Nguyen, K. (2023). Effective use of biochar as an additive for alkali-activated slag mortar production. *Construction and Building Materials, 370,* 130487.
15. Ahmadi, Z., Behfarnia, K., Faghihian, H., Soltaninia, S., Behravan, A. et al. (2023). Application of pervious alkali-activated slag concrete to adsorb runoff contaminants. *Construction and Building Materials, 375,* 130998.
16. Sharma, R., Pei, J., Miah, M. J., Jang, J. G. (2023). Effect of sillimanite sand on the mechanical property and thermal resistance of alkali-activated slag mortar. *Construction and Building Materials, 370,* 130654.
17. Reddy, K. C., Kim, G. M., Park, S. (2022). Modeling the phase evolution in alkali-activated slag cements upon interaction with seawater. *Case Studies in Construction Materials, 17,* e01476.
18. Ghiasvand, E., Mohammadi, H., Rezaei, Z., Ayyoubi, M., Dehghani, S. (2023). Evaluation of the durability of concretes containing alkali-activated slag exposed to the alkali-silica reaction by measuring electrical resistivity. *Construction and Building Materials, 367,* 130094.
19. Smirnov, V. G., Manakov, A. Y., Dyrdin, V. V., Ismagilov, Z. R., Mikhailova, E. S. et al. (2018). The formation of carbon dioxide hydrate from water sorbed by coals. *Fuel, 228,* 123–131.
20. Shah, J. (2000). Laboratory characterization of controlled low-strength material and its application to construction of flexible pipe drainage system. *Health Manpower Management, 19,* 30–59.
21. Yang, J., Huang, J., Su, Y., He, X., Tan, H. et al. (2019). Eco-friendly treatment of low-calcium coal fly ash for high pozzolanic reactivity: A step towards waste utilization in sustainable building material. *Journal of Cleaner Production, 238,* 117962.
22. Peng, L., Yang, J., Wang, H., Jin, X. (2022). The influence of CO_2 curing on the mechanical performance and the corresponding chloride ion resistance of alkali-activated compound mineral admixtures. *Coatings, 12,* 1920.
23. Sun, H., Cheng, W., Xu, H., Cai, Z., Yin, M. et al. (2023). Influence of CO_2 curing on the alkali-activated compound mineral admixtures' corrosion resistance to NaCl Dry-Wet alternations. *Coatings, 13(1),* 67.
24. Celikten, S., Sarldemir, M., Deneme, I. O. (2019). Mechanical and microstructural properties of alkali-activated slag and slag + fly ash mortars exposed to high temperature. *Construction and Building Materials, 217,* 50–61.
25. Wang, H., Jin, K., Zhang, A., Zhang, L., Han, Y. et al. (2021). External erosion of sodium chloride on the degradation of self-sensing and mechanical properties of aligned stainless steel fiber reinforced reactive powder concrete. *Construction and Building Materials, 287,* 123028.
26. Ahmadi, Z., Behfarnia, K., Faghihian, H., Soltaninia, S., Behravan, A. et al. (2023). Application of pervious alkali-activated slag concrete to adsorb runoff contaminants. *Construction and Building Materials, 375,* 130998.
27. Zhang, B., Tan, H., Shen, W., Xu, G., Ma, B. et al. (2018). Nano-silica and silica fume modifified cement mortar used as Surface Protection Material to enhance the impermeability. *Cement and Concrete Composites, 92,* 7–17.
28. Alrefaei, Y., Dai, J. (2022). Effects of delayed addition of polycarboxylate ether on one-part alkali-activated fly ash/slag pastes: Adsorption, reaction kinetics, and rheology. *Construction and Building Materials, 323,* 126611.
29. Li, S., Yang, J., Zhang, P. (2022). Hydration and hardening properties of reactive magnesia and Portland cement composite. *Construction and Building Materials, 327,* 126779.
30. Matějka, V., Sabovčík, T., Gryžbon, L., Vlček, J. (2022). Alkali activation of ground granulated blast furnace slag and low calcium fly ash using "one-part" approach. *Journal of Sustainable Metallurgy, 8,* 511–521.
31. Marple, M., Koroglu, B., Morrison, K., Crowhurst, J., Balachandra, A. et al. (2022). Accelerated carbonation and structural transformation of blast furnace slag by mechanochemical alkali-activation. *Cement and Concrete Composites, 156,* 106760.
32. Qaidi, S. M. A., Tayeh, B. A., Ahmed, H. U., Emad, W. (2022). A review of the sustainable utilisation of red mud and fly ash for the production of geopolymer composites. *Construction and Building Materials, 350,* 128892.
33. Qaidi, S. M. A., Atrushi, D. S., Mohammed, A. S., Ahmed, H. U., Faraj, R. U et al. (2022). Ultra-high-performance geopolymer concrete: A review. *Construction and Building Materials, 346,* 128495.

34. Al-Tayeb, M. M., Aisheh, Y. I. A., Qaidi, S. M. A., Tayeh, B. A. (2022). Experimental and simulation study on the impact resistance of concrete to replace high amounts of fine aggregate with plastic waste. *Case Studies in Construction Materials, 17,* e01324.
35. Qin, L., Gao, X. (2019). Properties of coal gangue-Portland cement mixture with carbonation. *Fuel, 245,* 1–12.
36. Chao, L., Duy, H., Mitiku, D., Vu, A. (2019). Improving the strength and engineering properties of alkali-activated slag-rice husk ash paste at the early ages with addition of various magnesium oxide content. *International Journal of Structure Civil Engineering, 8(3),* 210–214.
37. Akeed, M. H., Qaidi, S., Ahmed, H. U., Faraj, R. H., Majeed, S. S. et al. (2022). Ultra-high-performance fiber-reinforced concrete. Part V: Mixture design, preparation, mixing, casting, and curing. *Case Studies in Construction Materials, 17,* e01363.
38. Qaidi, S. M. A., Tayeh, B. A., Zeyad, A. M., Azevedo, A. R. G. D., Ahmed, H. U. (2022). Recycling of mine tailings for the geopolymers production: A systematic review. *Case Studies in Construction Materials, 16,* e00933.
39. Qaidi, S. M. A., Tayeh, B. A., Isleem, H. F., Azevedo, A. R. G. D., Ahmed, H. U. et al. (2022). Sustainable utilization of red mud waste (bauxite residue) and slag for the production of geopolymer composites: A review. *Case Studies in Construction Materials, 16,* e00994.
40. Qaidi, S. M. A., Mohammed, A. S., Ahmed, H. U., Faraj, R. H., Emad, W. et al. (2022). Rubberized geopolymer composites: A comprehensive review. *Ceramics International, 48(17),* e00933.